RESEARCH PAPER

Green synthesis of Au doped ZnO Decorated Reduced Graphene Oxide Using Ceratophyllum Demersum L Leaf Extract for Photocatalytic Discoloration of Rhodamine B dye

Aseel A. Kadhem 1,2, Hassan A. Alshamsi 1*

ARTICLE INFO

Article History:

Received 10 September 2025 Accepted 02 November 2025 Published 01 January 2026

Keywords:

Au-ZnO/rGO Eco friendly Photocatalysis Rhodamine B ROS

ABSTRACT

In the current study, a facile green synthesis of gold nanoparticles (Au NPs) , reduced graphene oxide nanosheets (rGO NPs) and gold doped zinc oxide nanoparticles (Au-ZnO NPs), and gold doped zinc oxide decorated reduced graphene oxide nanocomposite (Au-ZnO/rGO) have been reported using Ceratophyllum demersum L.(CDL) leaf extract for synergistic photocatalytic discoloration of Rhodamine B dye. The synthesized samples were investigated via the X-ray diffraction (XRD), Fourier-transform infrared spectroscopy (FTIR), UV-Vis diffuse reflectance spectroscopy (DRS), Field emission scanning electron microscopy (FE-SEM), Transmission electron microscopy (TEM), and Brunauer-Emmett-Teller (BET). The characterization results show that CDL exhibits a promise reducing and stabilizing properties for the fabrication of Au-ZnO/rGO nanocomposite where the Au and ZnO NPs were sufficiently distributed on the rGO Ns. In addition, the results showed that the biosynthesized Au-ZnO/rGO has a folded spherical morphology with the mean particle size of about 24.35 nm. Furthermore, Au doping sufficiently narrowed the ZnO bandgap, and loading on rGO nanosheets slow down the recombination of electron-hole pairs. The results of photocatalytic RhB discoloration showed that Au-ZnO/rGO nanocomposite exhibited the best efficiency and the discoloration rate reached 92.35 % under optimal conditions ([RhB]= 5 ppm, pH 9, catalyst dose=1.2 g/L, and irradiation time=180 min). RhB dye photocatalytic discoloration was evaluated using many ROS scavengers, which shows that the superoxide radical ('O₂-') plays a main in the discoloration reaction. In addition, after five cycles, the Au-ZnO/rGO nanocomposite retained 60.86 % of its initial activity.

How to cite this article

Kadhem A., Alshamsi H. Green synthesis of Au doped ZnO Decorated Reduced Graphene Oxide Using Ceratophyllum Demersum L Leaf Extract for Photocatalytic Discoloration of Rhodamine B dye. J Nanostruct, 2026; 16(1):169-187. DOI: 10.22052/JNS.2026.01.016

INTRODUCTION

Pollution of natural water sources due to the discharge of industrial exchange is a major global concern. The discharge of highly polluted water

* Corresponding Author Email: hassan.habeeb@qu.edu.iq

has certain damages not only on human health but also on the entire environmental system. In recent years, industries such as paper, textiles, food, paints, plastic, leather, cosmetics, medicines

¹ Department of Chemistry, College of Education, University of Al-Qadisiyah, Diwaniya, Iraq

² Ministry of Education, Waist Education Directorate, Kut city, Iraq

as well as petrochemicals are responsible for discharging synthetic organic dyes in rivers and groundwater [1]. Most of organic dyes in the liquid waste produced from the above industries are difficult to decompose due to their high chemical stability. Many traditional methods biological treatment, flotation, flocculation, precipitation, adsorption, aerobic, anaerobic, and electrochemical oxidation have been adopted for the treatment of industrial wastewaters; however, these methods cannot completely mineralize organic pollutants [2-7]. At present, one of the sufficient techniques is photocatalysis, a process in which ultra violet or visible light is obtained to assist the chemical degradation of a pollutant in the presence of a catalyst, which lowers the activation energy and enhancement the reaction rate [8,9].

Wide bandgap semiconductor materials such as zinc oxide (ZnO), titanium dioxide (TiO $_2$), molybdate (MoO $_4$), and tungstate (WO $_3$), have demonstrated to behave as effective photocatalysts [10,11]. However, ZnO nanoparticles are in the scientific spotlight because of their excellent properties like semiconducting, piezoelectric, optical, antibacterial characteristics, and promise photocatalytic activity [12].

ZnO is a wide band gap (3.37 eV) n-type semiconductor with a high exciton binding energy (60 eV). ZnO is actively employed as a base material in the fields of solar cells and photocatalysis [13,14]. The photocatalytic properties of ZnO can be greatly enhanced by controlling the fabrication conditions or forming hetero-nanostructures. However, disadvantages with using ZnO itself as a photocatalyst are well known. Specifically, the rapid electron-hole pair recombination rate, inefficient absorption of visible light, and poor adsorption capacity for organic pollutants. Currently, the main challenge to improve the efficiency of photocatalytic dye decomposition of ZnO is to slow down the recombination of photogenerated charge carriers (electron and holes). Hence, strategies such as heterostructuring, doping, and forming nanocomposites have been adopted to achieve this improvement [15]. One strategy to overcome the limitations of ZnO and improve its photoactive activity is to add different metals such as Pt, Pd, Ag and Au, etc. onto ZnO. Metal decoration on ZnO can act as an efficient electron acceptor and transporter, resulting in photoinduced

trapping of charge carriers, thus improving charge transfer processes and photocatalytic activity [16]. ZnO was subjected to effective modification procedures such as metal reduction on its surface to overcome the limitations of photocatalysis due to its large bandgap energy. It has been shown that gold nanoparticles enhance visible light absorption and charge separation in ZnO, which improves photocatalytic efficacy [17]. In addition, the formation of a nanocomposite with graphene-based ZnO improves the photocatalytic activity due to more efficient charge separation [18]. Specifically, reduced graphene oxide (rGO) offers new support in photocatalysis as proven by many studies. Graphene, a 2D material, is widely obtained in photocatalytic systems and can be used as an ideal catalyst due to its ultrafast electron mobility and excellent UV transmittance [19]. Additionally, its high specific surface area and abundant functional groups, for example, COOH make it a promise substrate for designing compounds using photocatalysts as metal oxides [20,21. Moreover, the adopting of graphene not only helps in enhancing adsorption capacity of the target pollutants on the photocatalyst surface, but also improves the transfer of photogenerated electron [22].

To synthesize metal oxides, several chemical and physical methods have been developed, including chemical vapor deposition, microwave irradiation, wet impregnation co-deposition, mechanical alloying, and green synthesis [23,24]. Among these methods, the green method remains the most nontoxic, cost-effective, and environmentally friendly. Biosynthesis, often known as green synthesis, has become a popular method for the synthesis of metal oxide nanostructures. The green reduction of noble metal ions and graphene oxide (GO) in the presence of metal oxides to obtain functional nanocomposites is a simple and facile method, which does not require high-energy consumption or advanced equipment [16, 25].

In this study, the facile green method was obtained to fabricate Au, rGO, Au-ZnO, Au-ZnO/rGO nanostructures using aqueous extract of eratophyllum demersum L leaves. The synthesized samples were studied with the techniques of X-ray powder diffraction (XRD), transmission electron microscopy (TEM), field emission scanning electron microscopy (FE-SEM), Fourier transform infrared spectroscopy (FTIR), and and UV-Vis diffuse reflectance spectroscopy (UV-Vis

DRS). Brunauer-Emmett-Teller (BET) method was used for a standard investigation of textural characteristics. The photocatalytic activity of the manufactured catalysts was investigated by observing the decrease in the color of Rhodamine B dye in an aqueous solution under visible light irradiation. The effect of irradiation time, catalyst dose, solution pH, and dye concentration on the photocatalytic discoloration efficiency of the dye was examined. The photocatalytic performance of the Au-ZnO/rGO nanocomposite was also investigated under optimal conditions in the presence of radical scavengers. The photocatalytic stability of the optimal catalyst was evaluated by recycling it several times. In view of the acquired findings, a suggested mechanism for the photocatalytic discoloration reaction of the dye has been presented.

MATERIALS AND METHODS

Chemicals

All chemicals were of high purity and handled as received without any further purification or treatment processes. Rhodamine B (empirical formula: $C_{28}H_{31}CIN_2O_3$, molecular weight: 479.01 g/mol, λ max = 553 nm), zinc nitrate

(Zn(NO₃)₂.6H₂O), hydrogen tetrachloroaurate (III) trihydrate (HAuCl₄.3H₂O), graphene oxide (GO, 15-20 sheets, 4-10% edge-oxidized), and isopropyl alcohol (IPA) were purchased from Merck. Ethylenediaminetetraacetic acid (EDTA) was received from NutriBiotic. Absolute ethanol (EtOH), ascorbic acid (AA) were supplied by Scharlau.

Preparation of aqueous leaf extract of CDL

The aqueous leaf extract of CDL leaf extract was prepared as previously reported [16]. Fresh CDL leaves were collected locally from River Al-Diwaniyah (southern Iraq). Typically, plant leaves were rinsed thoroughly first with tap water followed by distilled water (DW) to eliminate to eliminate dust and adherent particles. Afterward, the clean leaves were cut into small pieces and air-dried for a week at room temperature. The dried leaves were ground into a fine powder and sieved by using 100 µm size sieves. Afterward, 10 g of leaves powder were extracted by 100 mL of DW for 30 minutes at 70°C. Finally, the aqueous extract was filtered twice with Whatman No.1 filter paper, and the supernatant was stored in a glass container at 4°C for further processing.

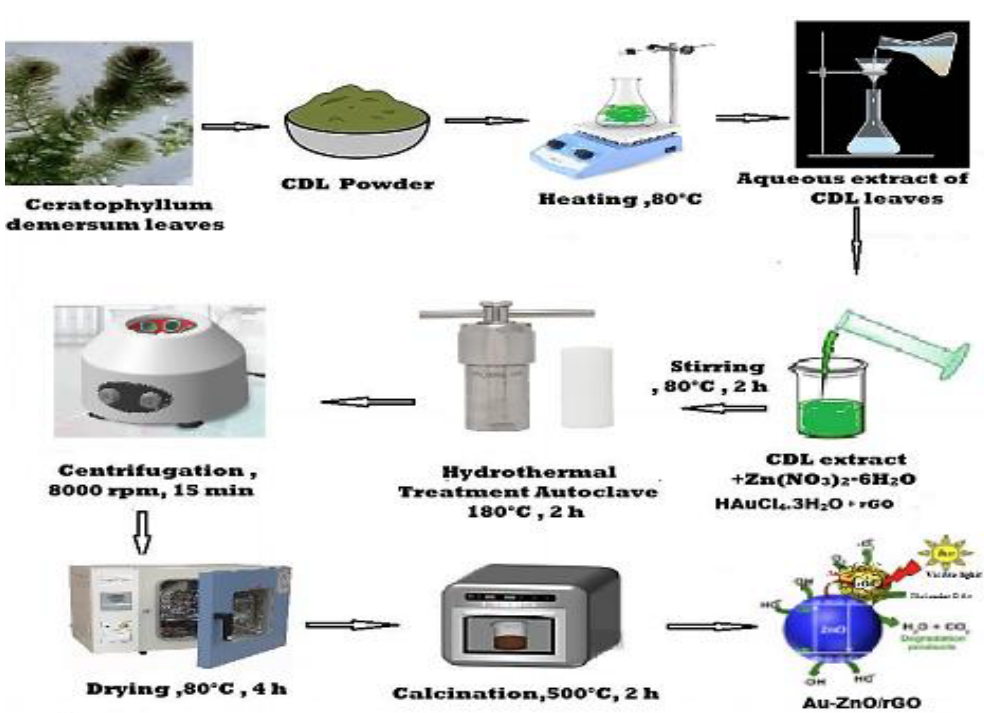


Fig. 1. Schematic showing biosynthesis flow of Au-ZnO/rGO nanostructure using CDL leaf extract.

Synthesis of rGO nanosheets

With slight modifications, the rGO Ns were prepared as previously reported [26]. Firstly, to obtain a homogeneous suspension, GO Ns (0.1g) were added to 50 mL of DW and sonicated for 20 min. Then, 50 mL of CDL extract was added with constant stirring at 80 °C for 2 h. Then, the suspension was transferred to a Teflon-lined stainless-steel autoclave and heated at 180 °C for further 2 h. Afterward, the rGO NPs were separated by centrifugation at 8000 rpm for 15 min and repeatedly washed with DW to remove any adsorbed impurities. Finally, the product was dried in a vacuum oven at 80 °C for 4 h.

Synthesis of Au NPs, Au - ZnO, and Au-ZnO/rGO

With some modifications, green synthesis of Au, Au - ZnO, and Au-ZnO/rGO NPs was conducted according to recently reported study [27]. Au NPs were synthesized using a green assisted hydrothermal process. Briefly, 0.1 g of AuHCl₄.3H₃O was added in DW (50 mL). To ensure complete it is dissolving, the solution was stirred for 24 h. Afterward, CDL extract (50 mL) was added while stirring at 80 °C for 2h. Then, the mixture was transferred to a Teflon-lined stainless-steel autoclave and heated at 180 °C for further 2 h. At this stage, the color of solution was changed from light brown to purple indicating the formation of Au NPs. Afterward; the Au NPs were separated by centrifugation at 8000 rpm for 15 min and repeatedly washed with DW to remove any unwanted impurities. Finally, the product was dried at 150 °C for 4 h.

To synthesis Au – ZnO (1 %) NPs, Zn(NO $_3$) $_2$.6H $_2$ O (2.97 g) was dissolved in 50 mL of DW followed by addition of AuHCl $_4$.3H $_2$ O (0.0393 g). Then, the same steps as described in synthesis of Au NPs were followed. To synthesis Au–ZnO/rGO nanocomposite, GO NPs (0.1g) was added to 50 mL of DW and sonicated for 20 min. Afterwards, Zn (NO $_3$) $_2$.6H $_2$ O (2.97 g) was added to GO suspension followed by addition of AuHCl $_4$.3H $_2$ O (0.0393 g). Then, the same steps as described in synthesis of Au NPs were followed. The Au – ZnO (1 %) and Au–ZnO/rGO samples were calcined for 2 h at 500 °C. The green synthesis method of Au–ZnO/rGO is shown in Fig. 1

Characterization

The crystallographic properties of the synthesized materials were investigated through

a powder X-ray diffraction (XRD) performed on a PANalytical X'Pert Pro using the Cu K α (with λ = 0.15405 nm) radiation in 2θ range of $10^{\circ}-80^{\circ}$. FT-IR spectra were conducted on a Bruker Vertex 80v within the wavenumbers range of 4000 – 400 cm⁻¹. The morphological characterization, particle shape and particle size of the synthesized samples were studied using a field-emission scanning electron microscope (TESCAN device, MIRA 3) and a transmission electron microscope (ZEISS Model EM10C-100 KV). Energy Dispersive X-ray Spectroscopy (EDX) was installed in the FE-SEM device to evaluate the elemental composition of the samples. The specific surface area (BET) and pore size (BJH) were evaluated from the N, adsorption/desorption isotherms at liquid nitrogen temperature, using a Quadrasorb SIMP. Shimadzu-Japan UV-Vis 160V spectrophotometer was employed to study the DRS-UV-Vis spectra at a range of 200-800 nm.

Photocatalytic performance

The photocatalytic efficacy of as synthesized photocatalysts in an aqueous solution was investigated using RhB dye a pollutant model. The photocatalytic discoloration of RhB was conducted in a Pyrex beaker using 100 W Xenon lamp as a visible light source. To achieve the adsorption/ desorption conditions, specific amount of catalyst was added to RhB solution (100 mL). The suspension was subjected to continuous magnetic stirring for 60 min in the dark at 298 K. Afterward, the suspension was continuously irradiated and stirred for 180 minutes. At specific time intervals, samples (2 mL) were withdrawn from the reaction vessel and centrifuged at 8,000 rpm for 20 min in order to remove the catalyst particles. The photocatalytic discoloration efficiency (PCD%) of RhB was calculated using Eq. 1 by measuring the absorbance at λ max of dye (553 nm) [17].

$$PDE\% = \frac{C_0 - C_t}{C_0} \times 100 \tag{1}$$

Where $\rm C_{o}$ represents the initial dye concentration and $\rm C_{t}$ represents the dye concentration at time (t). The effect of different factors, such as irradiation time (0-180 min), catalyst dosage (0.4-1.6 g/L), pH (3-11), and initial RhB concentration (5-20 ppm) were examined.

Scavenging investigation

To understand the photocatalytic discoloration

J Nanostruct 16(1): 169-187, Winter 2026

of RhB dye in detail, scavenging experiments of the reactive oxygen species (ROS) were performed during the reaction using the Au-ZnO/rGO NPs nanocomposite. The obtained inhibitors were isopropanol alcohol as a scavenger for hydroxyl radicals ('OH), ascorbic acid as a scavenger for superoxide radical anions ('O $_2$ '), and ethylenediaminetetraacetic acid as a scavenger for holes (h†) [16]. Under continuous stirring, 10 mM of scavenger was mixed with 100 mL of RhB dye solution (5 ppm) containing 0.12 g of Au-ZnO/rGO. The solution pH was adjusted to 11 and the temperature was fixed at 298K. After 180 minutes of illumination under visible light,the PCE% was determined using the Eq. 1.

Recycling study

The photocatalytic activity decreased due to the agglomeration of the photocatalyst particles. The use of Au-ZnO/rGO phoocatalyst was repeated five times at optimum conditions. After each recycling experiment, the catalyst particles were separated by centrifugation at 8000 rpm for 20 min and repeatedly washed with DW and ethanol. Afterward, the catalyst was dried at 80 °C using a vacuum oven for 4 h [9]. Then it used in a new cycle obtaining new fresh dye solution. After each reuse experiment, the PDE% was calculated using Eq. 1.

RESULTS AND DISCUSSION

Characterization of the synthesized materials

Table 1 Surface area analysis (BET, BJH) of rGO, ZnO, ZnO/rGO, Au, Au-ZnO, Au-ZnO-rGO.

| Property | rGO | Au NPs | Au-ZnO | Au-ZnO/rGO |
|--------------------|----------------|----------------|----------------|----------------|
| Surface area[m²/g] | 140.28 | 1.7470 | 14.3860 | 18.59 |
| Pore volume[m³/g] | 0.039 | 0.006260 | 0.037008 | 0.342452 |
| Pore diameter [nm] | 2.36 | 8.59 | 24.43 | 30.786 |
| Isothem type | IV | IV | IV | IV |
| Hysteres loops | H ₃ | H ₃ | H ₃ | H ₃ |
| Type of pore | Mesoporous | Mesoporous | Mesoporous | Mesoporous |

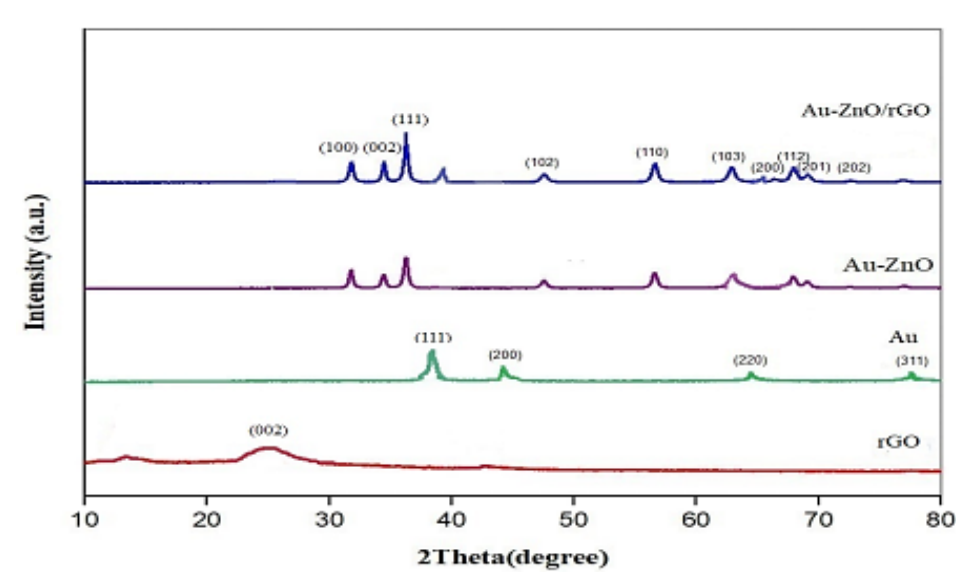


Fig. 2. XRD patterns for GO, Au, Au-ZnO, Au-ZnO/rGO.

X-ray Diffraction Analysis

In XRD analysis (Fig. 2), the XRD diffractogram of Au NPs indicates the presence of the four characteristic peaks at 38.15°, 43.97°, 64.53° and 77.39° which can be indexed to (111), (200), (220), (311) reflections of face centered cubic (FCC)

structure (JCPDS No. 65-8601) confirming that the green fabricated Au NPs were composed of pure crystalline Au metal [28]. The XRD pattern of Au-ZnO NPS exhibited two different sets of peaks associated with Au NPs. The first set of characteristic Bragg diffraction peaks belongs to

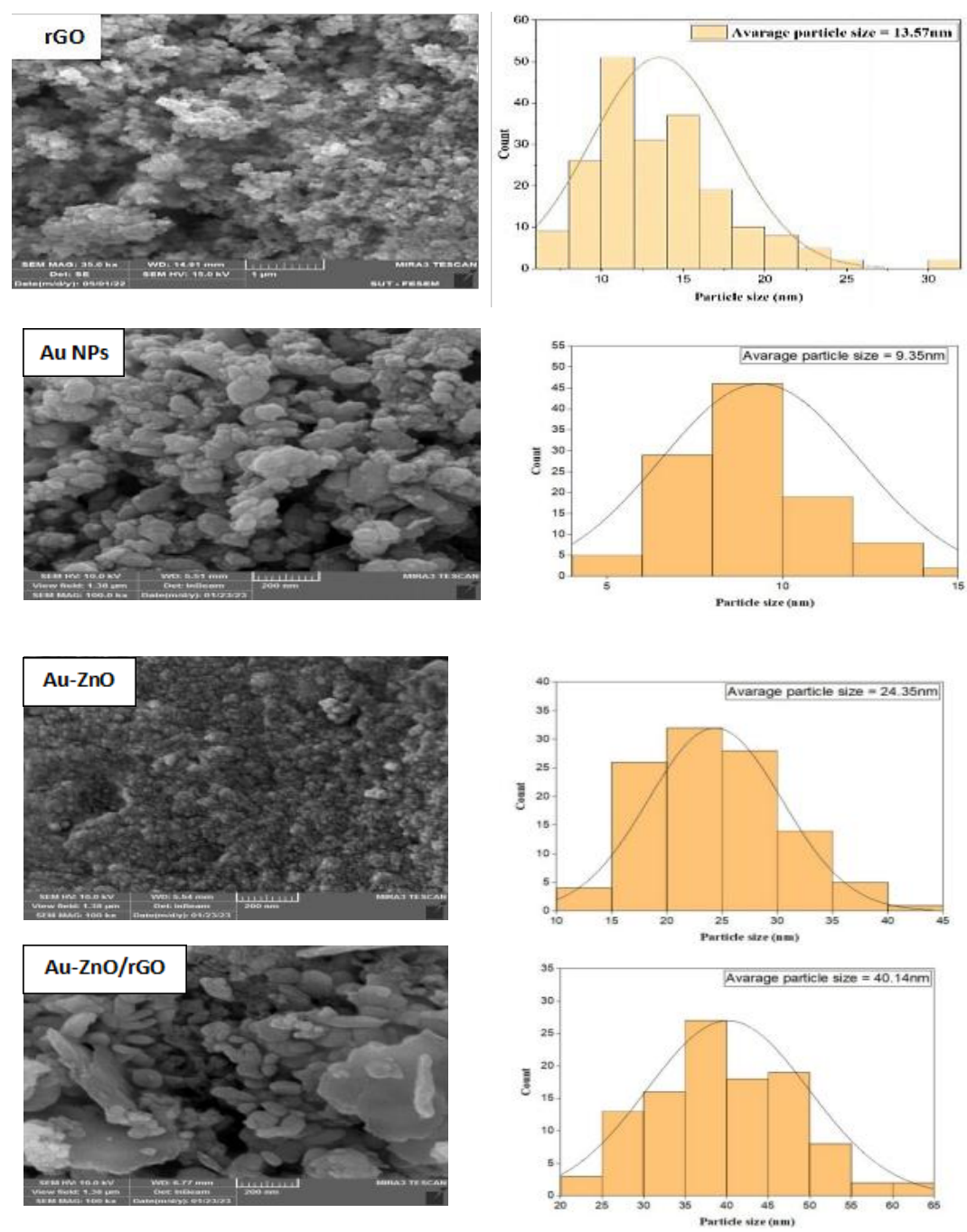


Fig. 3. FE-SEM images and corresponding histograms of particle size distribution of rGO, Au NPs, Au-ZnO and Au-ZnO/rGO.

ZnO NPs appearing at 2θ values of 31.81°, 34.44°, 36.24°, 47.51, 56.67°, 62.90°, 66.47°, 68.10° and 69.14° corresponding to 100, 002, 101, 102, 110, 103, 112, 200 and 201 Miller indices, respectively. All XRD peaks of ZnO NPs indicating the existence of ZnO with hexagonal wurtzite phase (JCPDS No. 361451) [18]. The second set peaks appearing at 38.17°, 43.94°, 64.47° and 77.42° assigned to lattice planes (111), (200), (220) and (311) confirms the inclusion of Au NPs in the nanocomposite. The XRD pattern of rGO sample exhibited the presence of a sharp diffraction peak at 2θ of 26.5 for the (002) plane, which it strongly confirms the formation of rGO with a highly disordered nature [29]. On the other hand, the XRD patterns of the Au-ZnO/ rGO sample showed a slight shift in the relevant peaks, which indicates that Au NPs, ZnO NPs and rGO Ns are included in the nanocomposite. The XRD analysis clearly confirming the absence of any external impurities in the four samples. The average crystallite size of synthesized materials was estimated using the Debye-Scherer equation. As listed in Table 1, the average crystallite sizes of Au, Au/ZnO, rGO, and Au-ZnO/rGO samples are 14.68, 20.91, 33.08 nm, respectively.

FE-SEM and EDX analysis

FE-SEM is a useful tool to investigate the

surface morphology and size distribution of the synthesized materials. Fig. 3 depicts FE-SEM images of the Au NPs having spherical morphology with few agglomerations indicating that CDL leaf extract acts as a promise-capping agent to separate the Au NPs from aggregation. The average particle size of the rGO was found to be 13.57nm, Au NPs was found to be 9.35 nm. FE-SEM image of Au/ ZnO NPs showed a denser spherical like shapes Au-ZnO NPs with an average size of 24.35 nm. This corresponds with the XRD analysis, which shows a decrease in the mean particle size with Au loading. The FE-SEM analysis of rGO demonstrate that the graphene sheets have a pattern-layered band wrinkled structure. In the Au-ZnO/GO sample, rGO sheets were successfully decorated with Au NPs and ZnO NPs. Furthermore, the Au-ZnO/rGO heterostructure shows a cross-linked flaky structure and excellent dispersion with few agglomerations. The FESEM results confirms the synthesis of heterostructure with sufficient simultaneous green reduction of Au(III) and GO sheets by the CDL leaf extract. In addition, these results suggest a uniform dispersion of Au and ZnO NPs on rGO NPs. The particle size distribution histogram of Au-ZnO/rGO shows that the average particle size of sample is 40.14 nm.

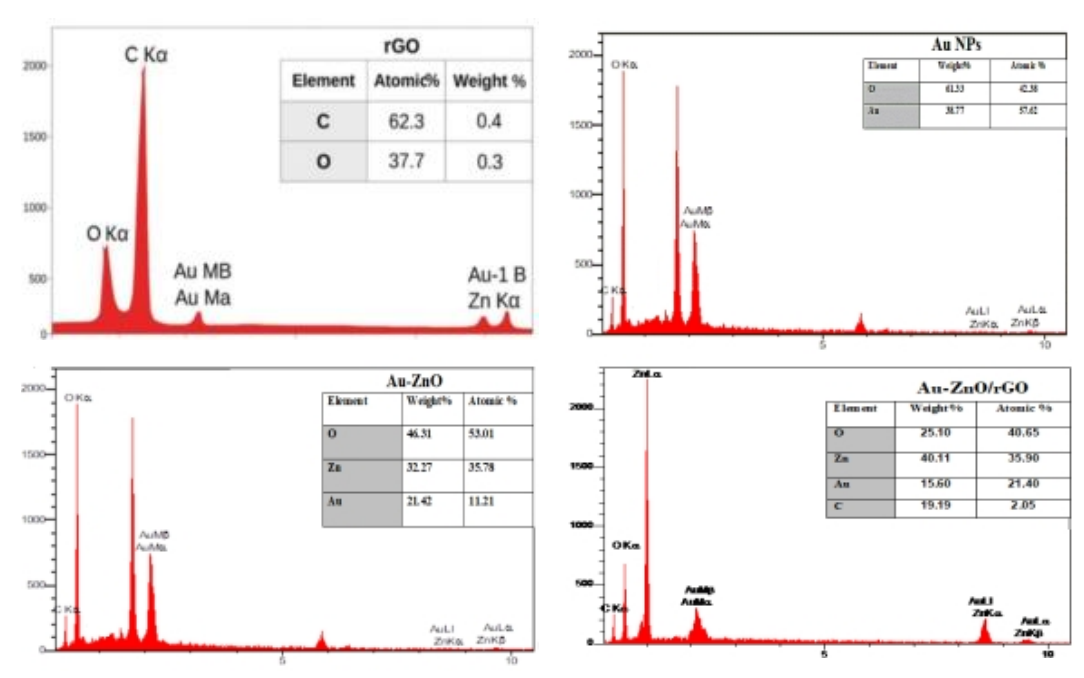


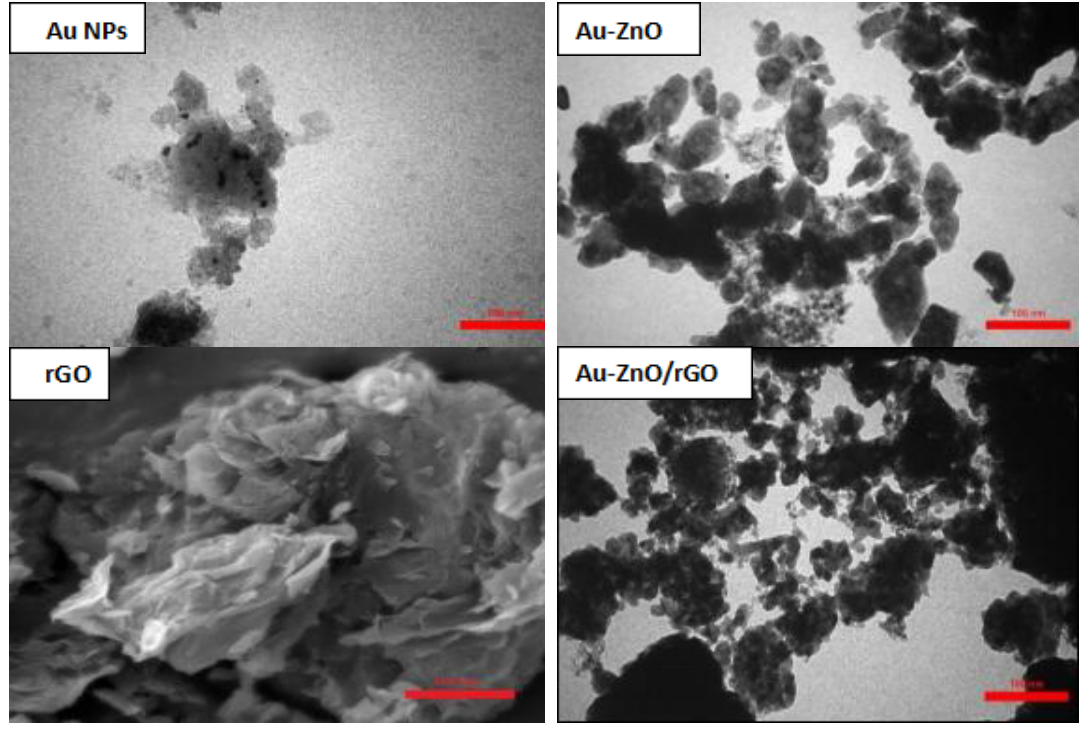
Fig. 4. EDX pattern for rGO, Au NPs, Au-ZnO and Au-ZnO/rGO.

The energy dispersive X-ray analysis (EDX) was conducted to examine the elemental composition of as synthesized materials. As Fig. 4 shows, the EDX of Au NPs exhibited the presence of Au and O elements. EDX spectrum depicted that 90.12% of the detected elements by this analysis correspond to Au. The EDX spectrum of Au-ZnO sample (Fig. 3) indicates that the nanocomposite is of an acceptable purity, where only Au, O and Zn elements were detected. As Figure shows, several elements were observed in the EDX spectrum of the Au-ZnO/rGO sample (Figure) including Au, C, Zn, and O were observed. This suggests the high purity of the synthesized Au-ZnO/rGO nanocomposite, which matches with XRD analysis. The spectrum of rGO (Figure) shows a higher composition ratio of carbon compared to oxygen (C = 61% and O = 39%). The high composition percentage of carbon to oxygen is due to the removal of the oxygen-containing functional groups from GO sheets during the green reduction process, indicating the formation of rGO Ns using CDL leaf extract.

Transmission Electron Microscopy (TEM)

The morphology and size of

phytosynthesized materials were investigated using TEM analysis, since Fig. 5 demonstrates the related TEM micrographs. TEM micrograph of rGO Ns reveals a thin and transparent layered rGO with few wrinkles on its surface. In addition, the edges of the sheets seemed to be smooth. In addition, TEM image revealed that the lateral sizes of rGO Ns have nano-scale sheets with folds and creases. TEM image of the Au NPs synthesized by the CDL leaf extract exhibited the existence of particles with various sizes and shapes. The Au NPs is uniform dispersed indicating that CDL acts as a successful reducing and capping agent with almost negligible aggregations occurred. TEM image of Au-ZnO exhibited the homogeneous distribution of Au NPs onto ZnO surface. These Au NPs are well dispersed, and these particles are seems like the spherical shape in nature. The obtained findings is in agreement with the results observed by Güler et al [29]. TEM image of Au-ZnO/rGO heterostructure confirms the anchoring Au and ZnO NPs on the rGO NPs. According to the TEM results, the uniform distribution of Au and ZnO particles on the graphene nanosheets can be observed. In general, no amorphous layers around Au, Au-ZnO, and Au-ZnO/rGO NPs were detected,



the

Fig. 5. TEM images of rGO, Au, Au-ZnO, and Au-ZnO/rGO.

indicating that during annealing process, most of organic species were successfully removed.

Surface area analysis (BET-BJH)

BET/BJH surface analysis is a very crucial test for surface area and porosity measurements of the fabricated nanomaterials. Fig. 6 depicts the N₂ gas adsorption-desorption isotherms and pore size distribution of the synthesized Au, rGO, Au-ZnO, and Au-ZnO/rGO materials. According to the IUPAC classification, all isotherms can be classified as near type IV isotherm, which is feature of the heterogeneous mesoporous materials possessing H3 hysteresis loop. The shape of these isotherms indicated the presence of an unrestricted multilayer formation process and the existence of slit-like mesoporous formed between aggregated nanoparticles [30]. As Table 2 shows, the total specific surface area of Au, rGO, Au-ZnO, and Au-ZnO/rGO are is 1.7470, 14.3860, and 18.59 m²/g, respectively. It is obvious that Au-ZnO/rGO nanohybrid have specific surface area more than Au and Au-ZnO samples. Such a result may be explained by the decline in the particles aggregation due to the presence of rGO sheets. The more specific surface area might lead to improved photocatalysis performance. This result was consistent with Mengistu et al [31]. Moreover, the pore diameter was measured to be 8.59, 24.43, and 30.786 nm for Au, rGO, Au-ZnO, and Au-ZnO/rGO, respectively. For Au-ZnO/rGO nanocomposite, BJH curve confirms the presence of the main mesoporous with diameters between 1 and 10 nm (pore volume, 0.342452 m³/g.

UV-vis diffuse reflectance spectra (UV-Vis DRS)

The UV-DRS measurements were conducted to evaluate light absorption features and the Au-doping and rGO adding influence on optical characteristics, including bandgap energy of Au-ZnO and Au-ZnO/rGO nanocomposites. ZnO is a wide-bandgap semiconductor with excellent activity UV light irradiation, which limits its

photocatalytic activity in the visible light region. The loading of metallic nanoparticles including Au, Ag, Pd, and Pt on the ZnO surface improves the optical characteristics and enhanced photocatalytic activity in the visible light range. Fig. 7 depicts the DRS curves and appraised bandgap for Au NPs, rGO NPs, Au ZnO NPs, and Au–ZnO/rGO nanohybrid. Estimation of band gap energy (Eg) is a vital issue for specification of the type of radiation light requested for photocatalytic degradation of pollutants. In the semiconductor, the absorption coefficient is the result of the incident photon energy. Near the absorption edge, the absorption coefficient for direct transition is given by following relationship [32]:

$$(\alpha h \upsilon)^2 = B(h \upsilon - E_g) \tag{2}$$

where α is the absorption coefficient, hv is the input photon energy, and B is the band tailing parameter. The presence of strong absorption peaks of ZnO in the ultraviolet region at the wavelength (371 nm) and through the curve, the gap energy of ZnO was calculated through Tuck's equation, and it amounted to (Eg = 3.3ev) [25]. For gold nanoparticles, its absorption edge near 549 nm. The UV-Vis absorption spectrum of the Au NPs usually exhibit an absorption peak, which is assigned to the localized surface plasmon resonance (LSPR) of Au NPs [33]. As shown in Figure, the position of the LSPR peak was detected at 549 nm. The doping of Au NPs significantly shifted the absorption edge of ZnO towards higher wavelengths at 440 nm due to the interfacial heterojunction between Au and ZnO. This suggest establishment of the p-type conductivity by the incorporation of Au ions into ZnO lattice sites leads to a narrowing bandgap [17]. In addition, the existence of oxygen vacancies makes impurity levels to be near the valence band, thereby enforcing the band gap narrowing. Moreover, in the Au-ZnO nanocomposite, the LSPR band of the Au NPs was observed in the visible spectral range,

Table 2. Band gap value of rGO, Au NPs, Au-ZnO, Au- ZnO/rGO.

| Sample | λmax (nm) | Band gap (eV) |
|------------|-----------|---------------|
| rGO | 523 | 2.37 |
| Au NPs | 549 | 2.26 |
| Au-ZnO | 440 | 2.8 |
| Au-ZnO/rGO | 477 | 2.9 |

at around 550 nm, which further indicates the doping of Au NPs in the Au-ZnO nanocomposite. The UV–Vis absorption spectrum of Au-ZnO/rGO composite show its absorption edge was shifted to

477 nm. It can be observed, that the doping of Au NPs and adding of rGO Ns causes a significant red shift in band edge absorption peak. The synergic interfacial interaction of Au NPs and rGO Ns could

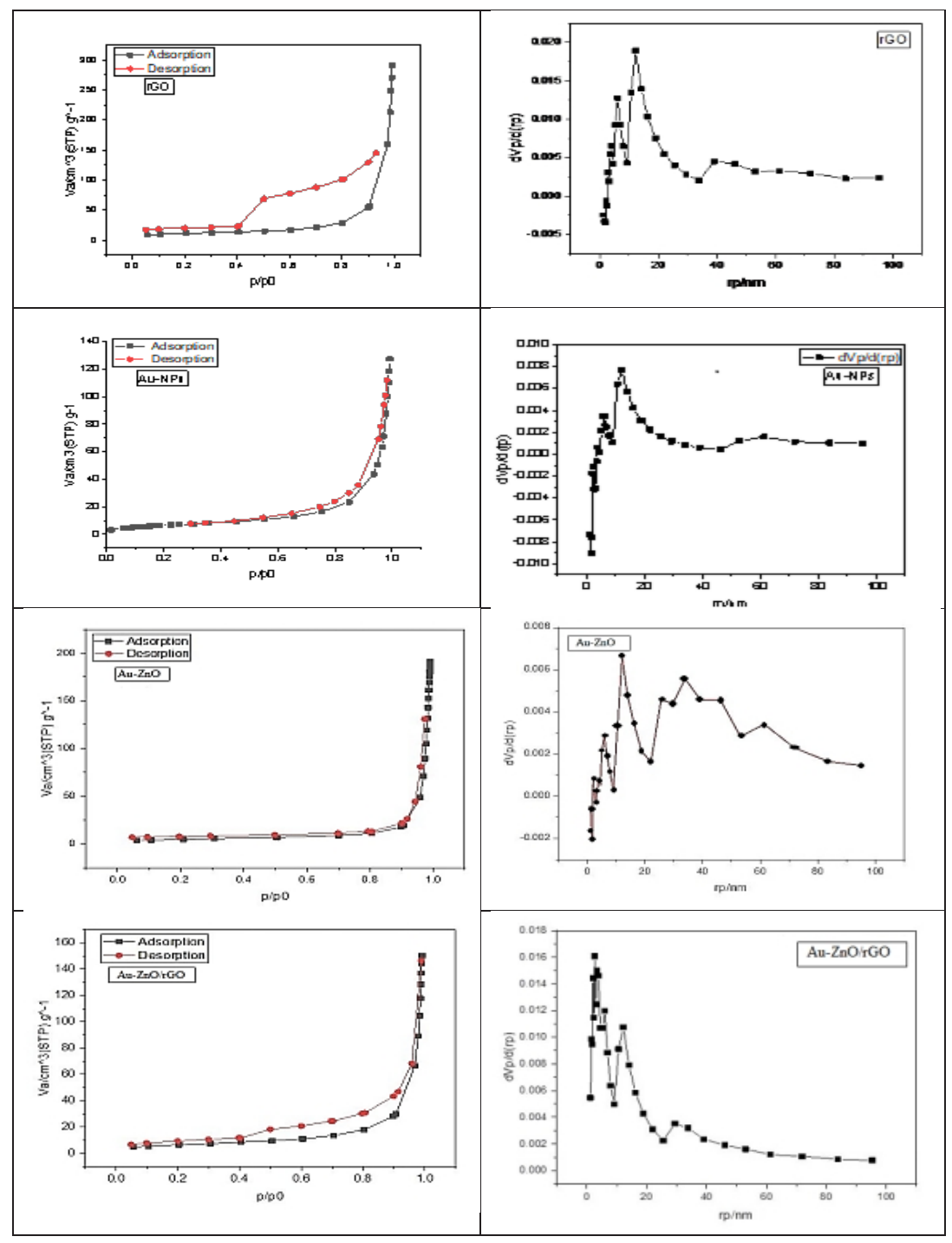


Fig. 6. N₂ adsorption/desorption isotherms and pore size distribution for synthesized materials.

narrowing the bandgap energy of ZnO. As Table 2exhibited, the estimated band gap of the Au, Au–ZnO and Au–ZnO/rGO were 2.26, 2.8, and 2.9 eV, respectively. In addition, the interfacial interaction between rGO and ZnO could eventuate in the band gap narrowing.

Fourier Transform Infrared Spectroscopy (FTIR)

FTIR spectroscopy was obtained further investigation the chemical structure of the synthesized materials, hence the FTIR spectra exhibit existence functional groups. As shown in Fig. 8, the broad peak was observed at 3440 cm⁻ ¹matches to the stretching vibration of alcoholic O-H, as well as carboxyl groups [34]. A weak narrow band that seen at 2927 cm⁻¹ indicates the presence of C-H stretched alkane groups. The band positioned at 1471 cm⁻¹ due to the N–O symmetric stretching of nitro groups. Weak band that observed at 1758⁻¹ is attributed to C=O stretching of COOH groups. Very weak band was detected 1049 cm⁻¹ corresponds to C–N stretched aromatic and aliphatic amines. In the FTIR spectrum of Au-ZnO sample, the broad band centered at 3440 cm⁻¹ is correspond to the characteristic stretching vibration mode of O-H group. The band centered at 440 cm⁻¹ assigned to stretching vibration of Zn-O bond [27]. More number of functional groups was present in Au–ZnO/rGO nano hybrid. The rGO spectrum shows a broad strong band at 3490 cm⁻¹ belongs to O-H stretching of the hydroxyl group. Compared to Au NPs and Au ZnO NPs, the disappearance characteristic absorption peak of C=O in the Au-ZnO/rGO composite obviously indicates the successful reduction of GO NPs [265]. Slight shift from 440 cm⁻¹ to 445 cm⁻¹ of Zn-O vibration mode can be observed. The peak at 1610 cm⁻¹ is corresponding to the in-plane vibration mode of the C=C skeleton. These findings in FTIR spectrum clearly confirm that Au-ZnO/rGO was successfully fabricated.

Photocatalytic discoloration of RhB dye

The photocatalytic discoloration of RhB in the presence of synthesized nanomaterials was investigated under visible light irradiation. A serest of parameters, namely illumination time, catalyst dose, initial concentration of dye, and solution pH were studied. In addition, experiments were performed to show the reactive species radical primarily responsible for the photocatalytic discoloration reactions. To demonstrate the economic feasibility of the best catalyst, its PCE%, and physicochemical properties were examined by conducting a reuse study. Absorption spectra were measured at specific intervals using a UV-Vis spectrometer for all experiments.

Catalyst type effect

The photocatalytic activity of the all synthesized samples against the cationic RhB dye is shown in Fig. 9. After 180 min of visible light irradiation, 60.57%, 45.78% and 26.43 of RhB were discolored using rGO NPs, Au NPs, Au-ZnO NPs, and Au-ZnO/rGO NPs, respectively. According to Fig. 10, the loading of ZnO NPs with Au NPs and rGO NPs enhanced an increase in the photocatalytic activity on the RhB discoloration under visible light illumination. This can be explained, due the fact that the Au NPs can act as electron traps facilitating

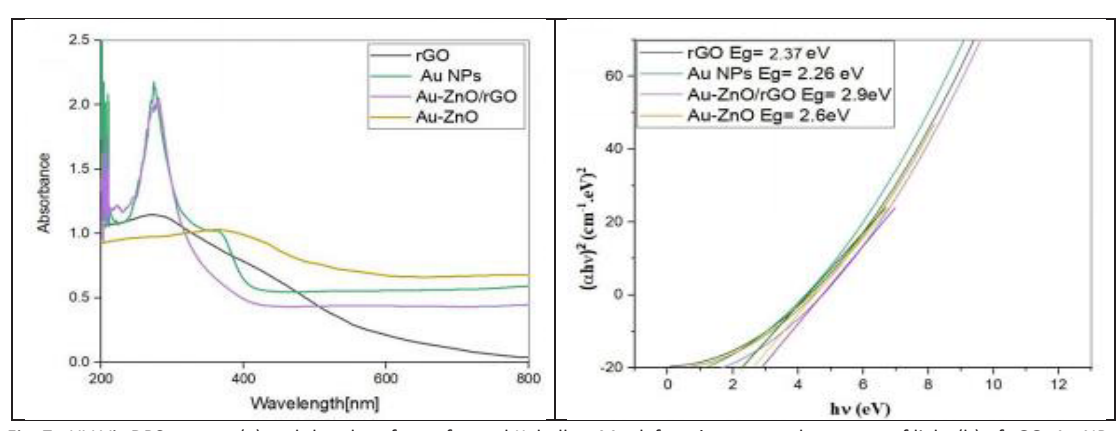


Fig. 7. UV Vis DRS spectra (a) and the plot of transformed Kubelka— Munk function versus the energy of light (b) of rGO, Au NPs, Au-ZnO, Au-ZnO/rGO.

the electron hole separation and subsequent transference of trapped electrons to the absorbed O_2 acting as an electron acceptor on the surface of ZnO NPs. Furthermore, besides the improving interfacial charge transfer, the incorporating of rGO Ns helps in enhancing adsorption capacity of the dye molecules on the catalyst surface, and enhances the transfer of photogenerated electron [35]. Thus, more molecules are loaded on the surface of Au-ZnO/rGO NPs, improving the photoexcited electron to the conduction band and simultaneously increasing the electron transfer

to the adsorbed O₂. The high surface area of rGO can contribute to the effective adsorption of RhB molecules on the catalyst surface. In addition, doping of Au NPs generates a band level very close to the ZnO CB edge. In general, both rGO NPs and Au NPs play synergistic roles in improving the catalytic properties of ZnO.

Catalyst dose effect

As photocatalytic activity is greatly influenced by the available active sites, so the main discoloration factor for RhB dye removal is catalyst dose. As

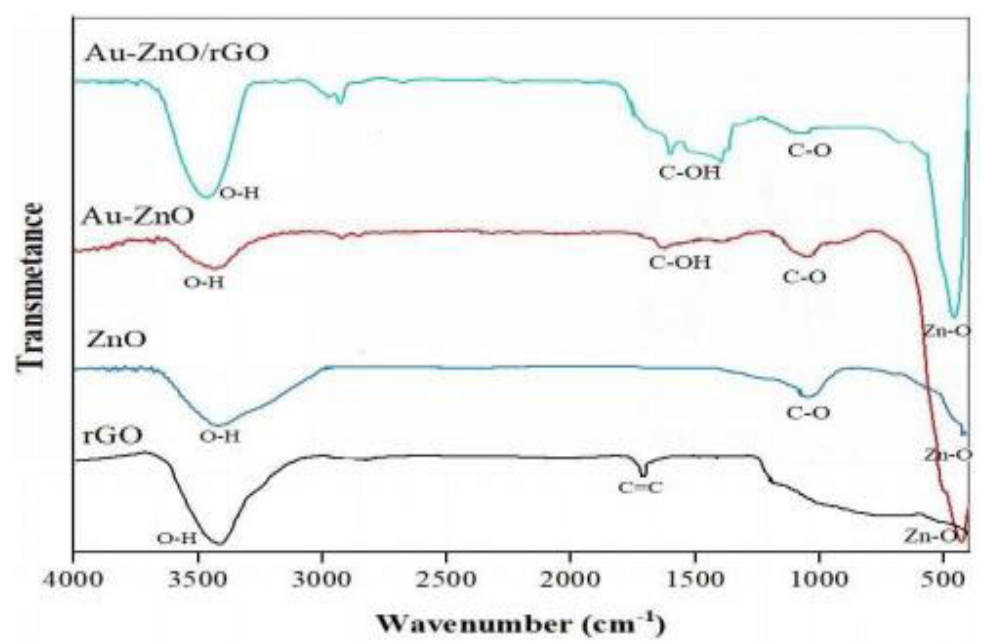


Fig. 8. FTIR spectra for Au, rGO, Au-ZnO, Au-ZnO/rGO.

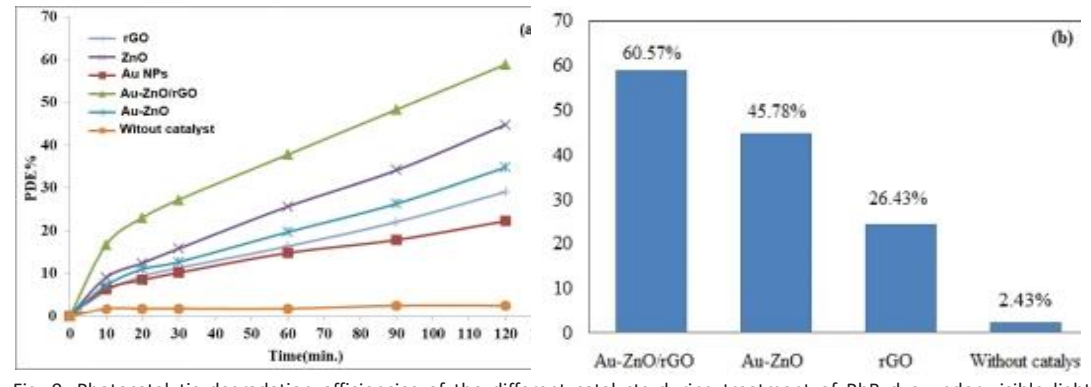


Fig. 9. Photocatalytic degradation efficiencies of the different catalysts during treatment of RhB dye under visible light illumination as a function of irradiation time (a) and catalyst type (b). (Catalyst dose = 1.0 g/L, [RhB]=10 ppm, pH=7 T= 298 K, irradiation time =180 min).

illustrated in Fig. 10, for varied Au-ZnO/rGO doses changing from 0.4 g/L to 1.2 g/L for a 10 ppm RhB concentration, the PDE% increased from 21.36 % to 50.70, respectively. It was observed that when the catalyst dose was increased, the Au-ZnO/rGO nanocomposite exhibited best photocatalytic activity. Maximum photocatalytic discoloration efficiency (52.72%) achieved with 1.4 g/L of the catalyst dosage.. As the catalyst dose increases to 1.2 g/L, the PDE% tends to be stable at higher dose (1.4 g/L). It was clear that a catalyst dose of 1.2 g/L was optimal for photocatalytic discoloration pf RhB dye. In general, an increase in catalyst dose causes an increase in the total surface area resulting in an increase in the adsorption of RhB molecules on the catalyst surface. In addition, the increase in catalyst dose increased the number of active sites on the photocatalytic surface, which in turn, enhance the number of reactive oxygen species, resulting in an improvement of photocatalytic activity [36]. No further increase in the photocatalytic activity could be observed beyond the optimum dose, though the number of active sites increases the penetration of light decreases due to shielding effect, which attributed to the agglomeration of photocatalyst particles.

Solution pH effect

The solution pH plays a vital role in the photocatalytic reactions, due to it controls the reactions during the removal of pollutants and beside the production of hydroxyl radicals also depends on the solution ph. The more important fact, effect of pH can be explored in terms of

electrostatic interaction between the pollutant molecules and catalyst surface. As shown in Fig. 11, the impact of pH on the photocatalytic discoloration of RhB was investigated the range of pH 3-11 in presence of Au-ZnO/rGO photocatalyst was investigated under constant conditions (irradiation time = 180 min, catalyst dosage 1.2 g/L, dye concentration 10 ppm, and temperature 298 K). The solution pH was adjusted using HCl and NaOH. It has been observed that the dye discoloration is affected by the pH value of pH and PDE% was better in the alkaline media compared to acidic media. The results showed that the photocatalytic discoloration efficiency increases with an increase in the pH value. At lower pH value (pH = 2) the PDE% reached to 34.92%, when the pH value of dye solution increases to 11, the PDE% increases to 60.35%. In general, the catalyst surface will be charged negatively when pH more than point of zero charge (pH > pHzpc), and positively when pH< pHzpc [39]. The pHpzc of the catalyst was estimated to be 8.2. This means at pH < 8.2, the surface Au-ZnO-rGO has a net positive charge. On the other hand, at pH > 8.2, the catalyst surface has a net negative charge. Due to fact that RhB molecules is positively charged, whereas Au-ZnO/rGO, ZnO is negatively charged above pH 8.2, so the increasing in pH value more than 8.2 tends to modify the catalyst charge negative charges by adsorbing HO⁻ ions, which favors the formation of strong oxidant species, hydroxyl radicals (HO*), hence, the photocatalytic activity increased due to the increase of the electrostatic attraction between negative catalyst surface and cationic

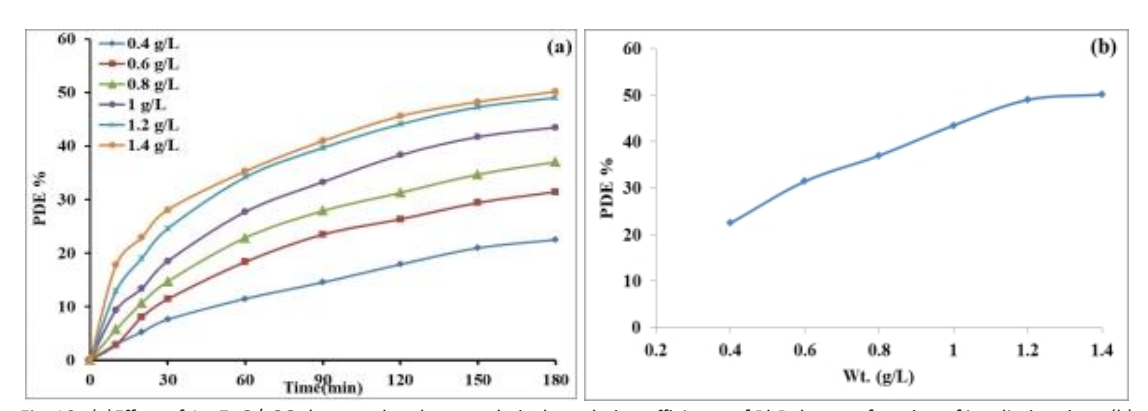


Fig. 10. (a)Effect of Au-ZnO/rGO dose on the photocatalytic degradation efficiency of RhB dye as a function of irradiation time, (b) relationship between PDE% and Au-ZnO/rGO dose. ([RhB]= 10 ppm, pH=7 T= 298 K, irradiation time =180 min).

dye molecules.

Initial dye concentration effect

Under the investigation of photocatalytic RhB discoloration, its initial concentration is very significant factor. The parameter of initial dye concentration was examined within the range of 5-10 ppm using 1.2 g/L of Au-ZnO/rGO at 298 K, pH 11 under 180 min of visible light irradiation. As shown in Fig. 12, the RhB dye solution with 5 ppm concentration exhibited maximum photocatalytic discoloration efficiency of 92.35 %. The color removal efficiency was decreased from 92.35 % to 42.71% with increasing the concentration of dye from 5 ppm to 20 ppm. Similar results were found previously for photocatalytic degradation RhB dye [37]. The reason behind this observation is due to as the initial dye amount was increased; the excess of dye molecules will be adsorbed on the catalyst surface, which in return reduces the active sites of the catalysts. In addition, it may be attributed to the decreasing of light penetrating power, when the initial dye concentration is increased, which reduces the production of photogenerated electrons holes pairs, hence ultimately leads to lowering the rate of photocatalytic activity [38]. Thus, O₂ and OH adsorption on the catalyst surface will reduces which in return reducing ROS formation, including powerful oxidizing agents O, and OH.

Kinetic study

Recent reports on the photocatalytic process have been investigated dye concentration depended degradation or discoloration kinetics. To study the kinetics of photocatalytic discoloration of RhB, the Langmuir—Hinshelwood kinetics model (pseudo-first-order kinetic model) as expressed

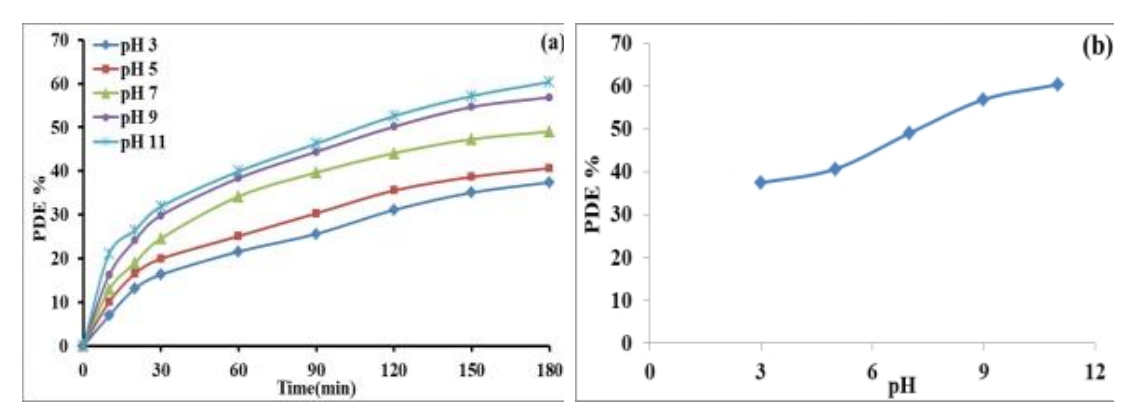


Fig. 11. The impact of initial pH on the effectiveness of RhB dye's photocatalytic degradation, (a) PDE% as a function of irradiation time (b) PDE% as a function of pH. ([RhB]= 10 ppm, dose = 1.2 g/L, T= 2980 K, irradiation time =180 min).

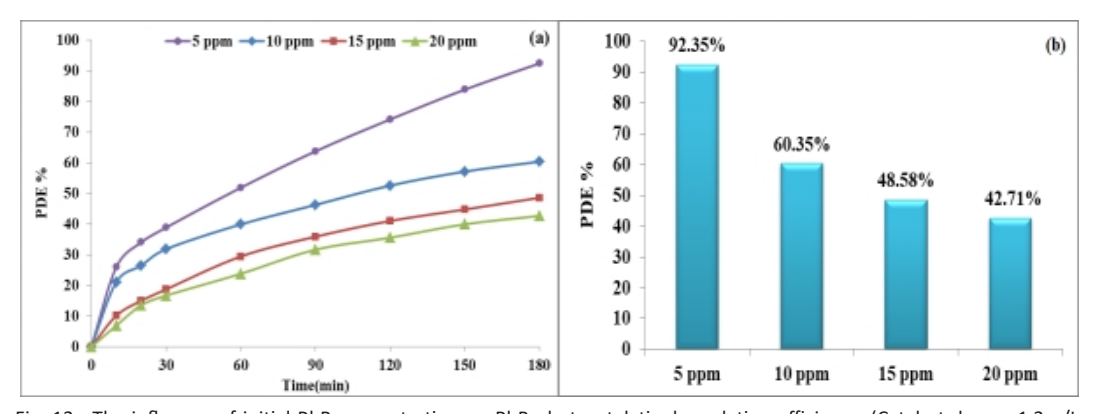


Fig. 12. The influence of initial RhB concentration on RhB photocatalytic degradation efficiency. (Catalyst dose = 1.2 g/L, pH=11, T= 2980 K, irradiation time =180 min).

in the Eq. 3 was obtained. The results in Fig. 13 were adjusted according to the pseudo- first-order kinetic model to determine the reaction rate constants.

$$ln \frac{(C_0)}{C_t} = kappt$$
(3)

Where C_0 represents the initial RhB concentration, C_t is the initial RhB concentration at (t) time, and k is the apparent first-order reaction rate constant (min⁻¹). The observed linear plots of $ln(C_0/C_t)$ versus irradiation accompanied with correlation coefficient (R²) values proves the applicability of pseudo first order kinetic

model for RhB dye discoloration over its various primary concentrations. In addition, it could be determined that pseudo-first-order rate constants of low concentration were significantly higher than for high concentration in the photocatalytic discoloration of dye. The kinetic study revealed that the photocatalytic discoloration of RhB dye in aqueous medium is significantly depends on the dye concentration, since, the dye degradation rate decreases with increasing initial concentration of RhB.

Recycling study

Recycling of the catalyst is one of the most important features of any heterogeneous

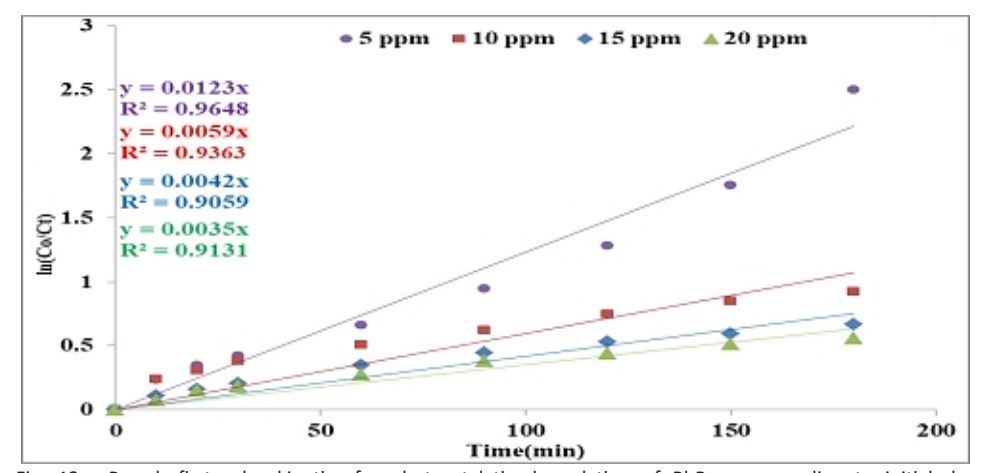


Fig. 13. Pseudo-first-order kinetics for photocatalytic degradation of RhB corresponding to initial dye concentration. (Catalyst dose = 1.2 g/L [RhB]= 5ppm, pH=11, T= 298 K, irradiation time =180 min).

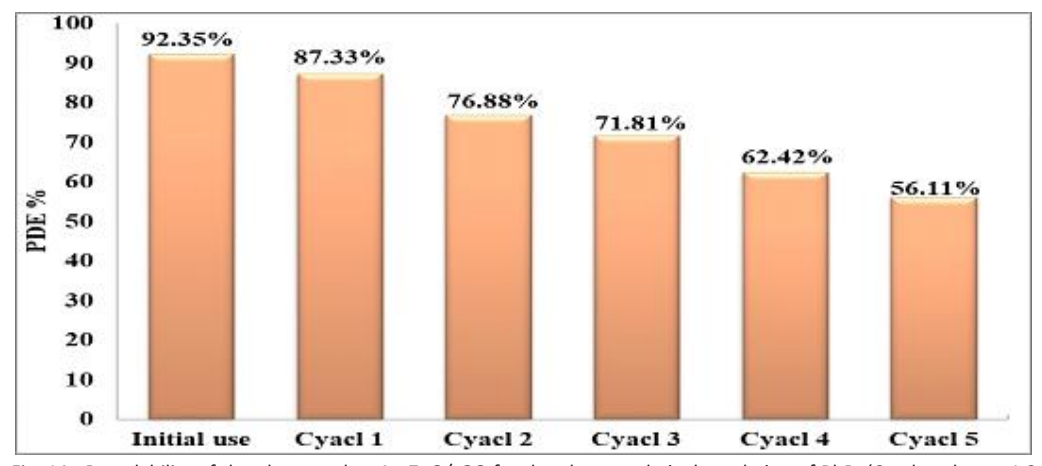


Fig. 14. Recyclability of the photocatalyst Au-ZnO/rGO for the photocatalytic degradation of RhB. (Catalyst dose = 1.2 g/L, [RhB] = 5 ppm, pH=11, T= 298 K, irradiation time =180 min).

catalyzed reaction since it is concerning to the costeffectiveness and feasibility of the catalyst. Fig. 14 depicted the reusability and stability of Au-ZnO/ rGO catalyst after five successive cycles within 180 min under visible light illumination. With constant conditions [RhB] = 5 ppm, pH 11, catalyst dosage = 1.2 g/L, T = 298 K), all cycles were conducted. As the results display, the photocatalytic activity of the Au-ZnO/rGO shows a gradual decline which revealed that the catalyst retained about 60.86 % of its initial reactivity under exposure to visible light radiation, where after five runs, the PDE% decreased from ~92.35% to 56.11%. This indicate that the Au-ZnO/rGO catalyst was reusable and exhibited acceptable potential on the application of wastewater remediation. The decrease in photocatalytic discoloration efficiency may be related with the occupation of active sites via adsorption of byproducts onto the catalyst surface. In addition, the decrease in photocatalytic activity may be due to the agglomeration of catalyst NPs during the recovery and washing processes, as previous studies have reported [39]. FTIR, XRD, and FESEM analyses (Fig. 15a-d) for the reused sample were performed. The XRD and FTIR analyses demonstrated no alteration in the crystalline and chemical nature of the reused catalyst after recycling for five runs could be observed. FESEM images clearly how that the catalyst surface has become smoother after recycling process. The reason may be due to the agglomeration of catalyst particles and decreasing surface area. The crystalline, chemical and morphological properties of reused Au-ZnO-rGO catalyst indicating a fair stability after multiple cyclic discoloration experiments.

Scavenging study

The addition of IPA led to the most significant drop in PDE%, confirming the major role of hydroxyl radicals [40]. Ascorbic acid and EDTA also reduced activity but to a lesser extent. As depicted in Fig. 16, it could be obviously noticed that the discoloration efficiency was poorest with

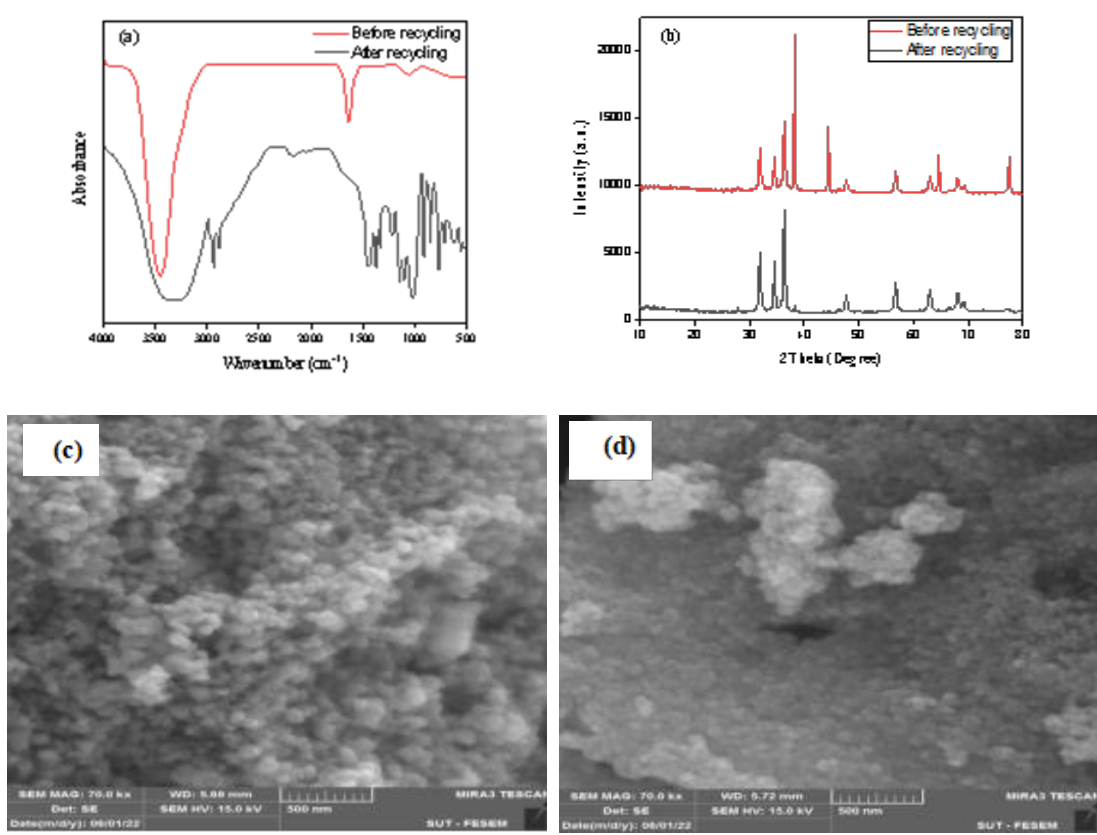


Fig. 15. (a) FTIR spectra of Au-ZnO/rGO before and after recycling, (b) XRD patterns of the Au-ZnO/rGO before and after recycling, (c) FESEM image of Au-ZnO/rGO before recycling, and (d) FESEM image of Au-ZnO/rGO after recycling.

isopropanol addition (7.12%), followed by EDTA (41.69%) and ascorbic acid addition (58.75%), compared with the performance by Au-ZnO-rGO catalyst without any scavenger addition (92.35%). The results present that the *OH radicals are mainly responsible for the photocatalytic degradation of RhB dye under visible light irradiation.

Mechanism of photocatalytic reaction

Under visible light, Au facilitates plasmoninduced electron excitation, injecting electrons into the ZnO conduction band. rGO acts as an electron shuttle, minimizing charge recombination and prolonging ROS generation [17,28]. The sequence involves photon absorption and e^-/h^+ generation, electron transfer, O_2 reduction to O_2^- and subsequent *OH formation, and then RhB degradation via ROS. The resulting holes can interact with hydroxide ions (OH·) and water molecules (H₂O) to generate hydroxyl radicals (OH.) which regarded as strong oxidizing agents [41]:

$$Au-ZnO/rGO(h^+) + H_2O \longrightarrow Au-ZnO/rGO(OH^+) + H^+$$

A reaction can occur between photogenerated electrons and electron acceptors such as molecular

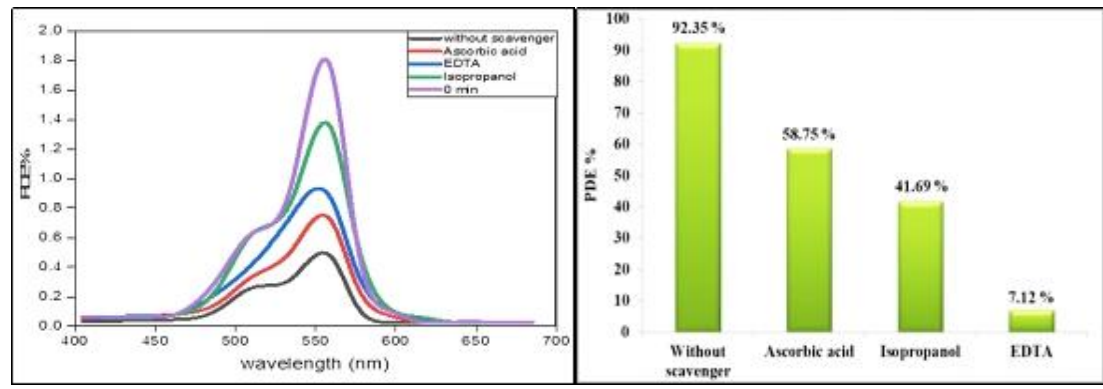


Fig. 16. PDE% as a function of scavenger type.

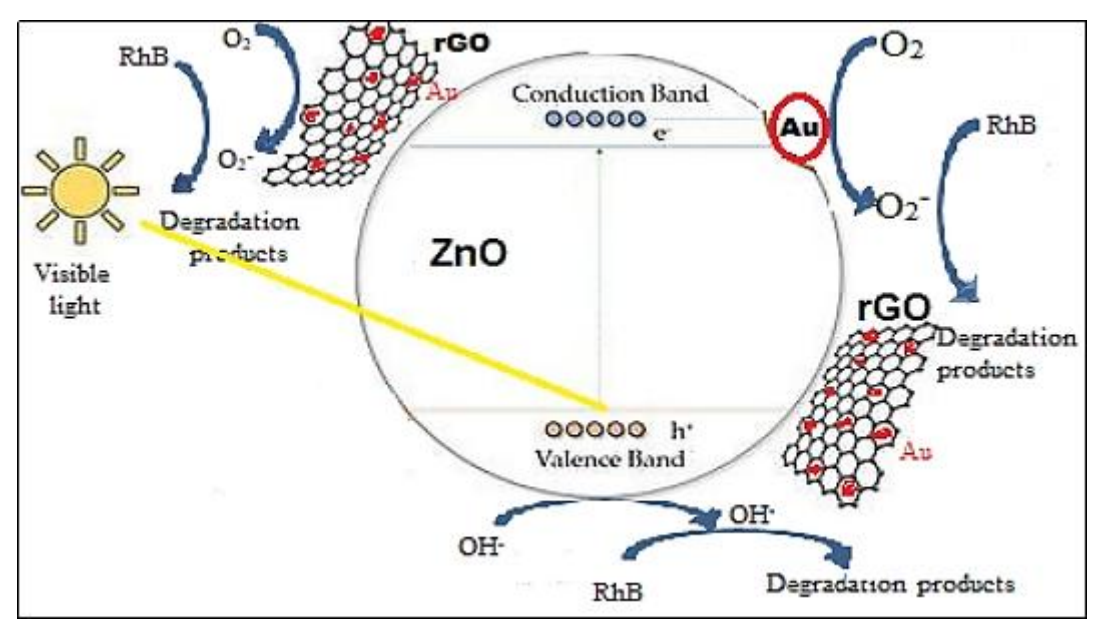


Fig. 17. Schematic diagram of the photocatalytic degradation of Rhodamine B dye using Au-ZnO/rGO nanocomposite.

oxygen adsorbed on the catalyst surface, where superoxide radicals are generated [42]:

$$Au-ZnO/rGO(e^{-}) + O_{2} \rightarrow Au-ZnO/rGO+({}^{\bullet}O_{2}^{-})$$
 (5)

It is also possible to oxidize RhB molecules through a self-sensing process by injecting electrons into the conduction band of Au-ZnO/rGO [41]:

$$dye + hv \rightarrow dye^*$$
 (6)

dye* + Au-ZnO/rGO
$$\rightarrow$$
Au-ZnO-rGO (e_{cb}- + h_{vb+})+ (d ye)⁺ (7)

Charge carriers and ROS play a synergistic role in the degradation and mineralization of the dye. [41, 43]:

Au-ZnO/rGO(OH
$$^{\circ}$$
)+dye/dye $^{*}\rightarrow$ Au-ZnO/rGO
+degradation products \rightarrow CO $_{2}$ + H $_{2}$ O (8)

$$Au-ZnO/rGO(^{\circ}O_{2}^{-})+dye/dye^{*} \rightarrow Au-ZnO/rGO+degradation products \rightarrow CO_{2}+H_{2}O$$
 (9)

$$Au-ZnO/rGO(h^+)+dye/dye^* \rightarrow Au-ZnO/rGO+degradation products \rightarrow CO_2+H_2O$$
 (10)

Fig. 17 schematically illustrates the proposed degradation mechanism of RhB by the Au–ZnO/rGO heterojunction, highlighting the synergistic roles of charge carriers and reactive oxygen species.

CONCLUSION

In the current work exhibits the possibility of utilizing the aqueous leaf extract of Ceratophyllum demersum L. for the biosynthesis of gold, reduced graphene oxide, gold doped- zinc oxide as well as gold doped- zinc oxide decorated reduced graphene oxide. The synthesized samples were characterized in structural, morphological, textural, and optical properties by XRD, FTIR FESEM, TEM, BET/BJH and UV-DRS technique. The crystalline structures of Au, Au-ZnO and Au-ZnO/rGO were confirmed. Moreover, EDS results indicated that the Au-ZnO/rGO sample was composed of Zn,O,C, and Au elements distributed homogeneously. Furthermore, bandgap of ZnO clearly decreased with Au doping and rGO loading, resulting in a broader visible light harvesting and better reduction of electronhole pairs recombination. The synthesized materials were investigated for their potential to discolor the Rhodamine B dye under visible light illumination. Compared to other samples, Au-ZnO/rGO nanocomposite showed of 92.35 % of dye discoloration within irradiation for 120 min irradiation.

ACKNOWLEDGMENTS

The authors are grateful to University of the Al Qadisiyah, College of Education for their support.

CONFLICT OF INTEREST

The authors declare that there is no conflict of interests regarding the publication of this manuscript.

REFERENCES

- Pereira AGB, Rodrigues FHA, Paulino AT, Martins AF, Fajardo AR. Recent advances on composite hydrogels designed for the remediation of dye-contaminated water and wastewater: A review. Journal of Cleaner Production. 2021;284:124703.
- Shamkhi HA, Albdiri ADZ, Jabir FA, Petruzzelli D. Removal of Pb²⁺, Cu²⁺, and Cd²⁺ Ions from a Saline Wastewater Using Emulsion Liquid Membrane: Applying Response Surface Methodology for Optimization and Data Analysis. Arabian Journal for Science and Engineering. 2021;47(5):5705-5719.
- Shamkhi HA, Albdiri ADZ, Jabir FA, Koter SS. Experimental and modeling studies on simultaneous extraction of Pb²⁺, Cu²⁺, and Cd²⁺ from diluted acidic aqueous solutions by emulsion liquid membrane. Chem Eng Commun. 2020;209(2):246-255.
- 4. Al-Hussainawy MK, Sahb Mehdi Z, Jasim KK, Alshamsi HA, Saud HR, Kyhoiesh HAK. A single rapid route synthesis of magnetite/ chitosan nanocomposite: Competitive study. Results in Chemistry. 2022;4:100567.
- Ječmenica Dučić M, Krstić A, Zdolšek N, Aćimović D, Savić B, Brdarić T, et al. Low-Cost Graphene-Based Composite Electrodes for Electrochemical Oxidation of Phenolic Dyes. Crystals. 2023;13(1):125.
- Lucas MS, Teixeira AR, Jorge N, Peres JA. Industrial Wastewater Treatment by Coagulation–Flocculation and Advanced Oxidation Processes: A Review. Water. 2025;17(13):1934.
- Kato S, Kansha Y. Comprehensive review of industrial wastewater treatment techniques. Environmental Science and Pollution Research. 2024;31(39):51064-51097.
- Al-Nayili A, Alhaidry WA. Novel surface structure of LaFeO3/ nitrogen-deficient g-C3N4 nanocomposites to improve visible-light photocatalytic performance toward phenol removal. Environmental Science and Pollution Research. 2024;31(6):8781-8797.
- Albusalih RH, Alshamsi HA. Enhancement of Photocatalytic Degradation of RhB Dye Using CuWO₄/ZnO/N-g-C₃N₄ Nanocomposite Under Visible Light Irradiation. J Cluster Sci. 2025;36(4).
- Ansari AS, Azzahra G, Nugroho FG, Mujtaba MM, Ahmed ATA. Oxides and Metal Oxide/Carbon Hybrid Materials for Efficient Photocatalytic Organic Pollutant Removal. Catalysts. 2025;15(2):134.
- 11. Yousif QA, Mahdi KM, Alshamsi HA. TiO2/graphene and MWCNT/PEDOT:PSS nanocomposite-based dye-sensitized solar cell: Design, fabrication, characterization, and investigation.

- Optik. 2020:219:165294.
- Zhu C, Wang X. Nanomaterial ZnO Synthesis and Its Photocatalytic Applications: A Review. Nanomaterials. 2025;15(9):682.
- Pratomo U, Fransisca N, Adzani MD, Irkham I, Sulaeman AP, Eddy DR, et al. Doping of rare earth element: The effects in elevated physical and optical properties of ZnO. Talanta Open. 2025;11:100411.
- Yousif QA, Mahdi KM, Alshamsi HA. Enhanced photovoltaic performance of dye-sensitized solar cell based on ZnO nanoparticles and ZnO/graphene nanocomposites. J Chin Chem Soc. 2021;68(9):1637-1643.
- Baig A, Siddique M, Panchal S. A Review of Visible-Light-Active Zinc Oxide Photocatalysts for Environmental Application. Catalysts. 2025;15(2):100.
- kadhem AA, Alshamsi HA. Biosynthesis of Ag-ZnO/rGO nanocomposites mediated Ceratophyllum demersum L. leaf extract for photocatalytic degradation of Rhodamine B under visible light. Biomass Conversion and Biorefinery. 2023;14(19):24655-24669.
- Abdulhusain ZH, Alshamsi HA, Salavati-Niasari M. Facile synthesis of Au/ZnO/RGO nanohybrids using 1,8-diamino-3,6dioxaoctan as novel functional agent for photo-degradation water treatment. Journal of Materials Research and Technology. 2021;15:6098-6112.
- Abdulhusain ZH, Alshamsi HA, Salavati-Niasari M. Silver and zinc oxide decorated on reduced graphene oxide: Simple synthesis of a ternary heterojunction nanocomposite as an effective visible-active photocatalyst. Int J Hydrogen Energy. 2022;47(80):34036-34047.
- Al-nayili A, Khayoon HA, Alshamsi HA, Cata Saady NM. A novel bimetallic (Au-Pd)-decorated reduced graphene oxide nanocomposite enhanced Rhodamine B photocatalytic degradation under solar irradiation. Materials Today Sustainability. 2023;24:100512.
- Altaee H, Alshamsi HAH, Joda BA. Reduced graphene oxide supported palladium nanoparticles as an efficient catalyst for aerobic oxidation of benzyl alcohol. AIP Conference Proceedings: AIP Publishing; 2020. p. 030036.
- Manikandan V, Lee NY. Reduced graphene oxide: Biofabrication and environmental applications. Chemosphere. 2023;311:136934.
- Dayekh NS, Al-Nayili A. Heterogeneous photocatalytic degradation of phenol over Pd/rGO sheets. AIP Conference Proceedings: AIP Publishing; 2022. p. 030010.
- Parashar M, Shukla VK, Singh R. Metal oxides nanoparticles via sol–gel method: a review on synthesis, characterization and applications. Journal of Materials Science: Materials in Electronics. 2020;31(5):3729-3749.
- 24. Alhalili Z. Metal Oxides Nanoparticles: General Structural Description, Chemical, Physical, and Biological Synthesis Methods, Role in Pesticides and Heavy Metal Removal through Wastewater Treatment. Molecules. 2023;28(7):3086.
- Liu X, Li X, Liu X, He S, Jin J, Meng H. Green preparation of Ag-ZnO-rGO nanoparticles for efficient adsorption and photodegradation activity. Colloids Surf Physicochem Eng Aspects. 2020;584:124011.
- Alshamsi HA, Ali SK, Alwan Altaa SH. Green Synthesis and Characterization of Reduced Graphene Oxide (RGO) using Sabdarriffa L extract and its Solubility Property. Journal of Physics: Conference Series. 2020;1664(1):012058.
- Albo Hay Allah MA, Alshamsi HA. Green synthesis of ZnO NPs using Pontederia crassipes leaf extract: characterization, their adsorption behavior and anti-cancer property. Biomass Conversion and Biorefinery. 2022;14(9):10487-10500.
- 28. Alshamsil HA, Nema QA, Alwan SH. Facile one-step synthesis

- of Au-ZnO/MWCNTs for photocatalytic treatment of Reactive Blue dye in aqueous solution. IOP Conference Series: Earth and Environmental Science. 2022;1029(1):012003.
- Güler AC, Antoš J, Masař M, Urbánek M, Machovský M, Kuřitka I. Boosting the Photoelectrochemical Performance of Au/ ZnO Nanorods by Co-Occurring Gradient Doping and Surface Plasmon Modification. Int J Mol Sci. 2022;24(1):443.
- S. Muniandy S, Mohd Kaus NH, Jiang Z-T, Altarawneh M, Lee HL. Green synthesis of mesoporous anatase TiO₂ nanoparticles and their photocatalytic activities. RSC Adv. 2017;7(76):48083-48094
- 31. Tamiru Mengistu M, Wondimu TH, Andoshe DM, Kim JY, Zelekew OA, Hone FG, et al. g-C₃N₄–Co₃O₄ Z-Scheme Junction with Green-Synthesized ZnO Photocatalyst for Efficient Degradation of Methylene Blue in Aqueous Solution. Bioinorg Chem Appl. 2023:2023:1-14.
- 32. Hamza AM, Alshamsi HA. Design of novel Z-scheme g-C₃N_a/TiO₂/CuCo₂O₄ heterojunctions for efficient visible light-driven photocatalyic degradation of rhodamine B. Sci Rep. 2024;14(1).
- 33. Yadav N, Chaudhary P, Dey KK, Yadav S, Yadav BC, Yadav RR. Non-functionalized Au nanoparticles can act as high-performing humidity sensor. Journal of Materials Science: Materials in Electronics. 2020;31(20):17843-17854.
- 34. Alshamsi HA, Jaffer AA. New Hibiscus Sabdariffa L petals extract based Green synthesis of zinc oxide nanoparticles for photocatalytic degradation of Rhodamine B dye under solar light. AIP Conference Proceedings: AIP Publishing; 2022. p. 040017.
- 35. Phor L, Kumar R, Khanna V, Menon SV, Singh A, Singh M, et al. Graphene and Cerium Oxide Nanocomposites: Pioneering Photocatalysts for Organic Dye Degradation from Wastewater. Processes. 2025;13(3):720.
- Asiri M, Sead FF, Mayani SV, Menon SV, Thakur R, Ray S, et al. Enhanced photocatalytic degradation of penicillin G using magnetic silica doped ZnAl- layered double hydroxides. Sci Rep. 2025;15(1)
- 37. Lops C, Ancona A, Di Cesare K, Dumontel B, Garino N, Canavese G, et al. Sonophotocatalytic degradation mechanisms of Rhodamine B dye via radicals generation by micro- and nano-particles of ZnO. Applied Catalysis B: Environmental. 2019;243:629-640.
- Hameed BH, Akpan UG, Wee KP. Photocatalytic degradation of Acid Red 1 dye using ZnO catalyst in the presence and absence of silver. Desalination and Water Treatment. 2011;27(1-3):204-209
- Abkar E, Al-Nayili A, Amiri O, Ghanbari M, Salavati-Niasari M. Facile sonochemical method for preparation of Cs2Hgl4 nanostructures as a promising visible-light photocatalyst. Ultrason Sonochem. 2021;80:105827.
- 40. de Quadros S, Horst Pereira Metz DC, Zimmermann LM. Efficient degradation of cationic dyes by ZnO and ZnO–Fe(III) quantum dots under natural sunlight and UV light. Journal of Physics and Chemistry of Solids. 2023;181:111464.
- Alwan SH, Salem KH, Alshamsi HA. Visible light-driven photocatalytic degradation of Rhodamine B dye onto TiO₂/ rGO nanocomposites. Materials Today Communications. 2022;33:104558.
- 42. González-Crisostomo JC, López-Juárez R, Petranovskii V. Photocatalytic Degradation of Rhodamine B Dye in Aqueous Suspension by ZnO and M-ZnO (M = La³+, Ce³+, Pr³+ and Nd³+) Nanoparticles in the Presence of UV/H₂O₂. Processes. 2021;9(10):1736.
- 43. Sellam M, Azizi S, Bouras D, Fellah M, Obrosov A, El-Hiti GA. Degradation of rhodamine B dye under visible and solar light on zinc oxide and nickel-doped zinc oxide thin films. Opt Mater. 2024;151:115316.